Adaption of artificial microvascular networks

Thierry Fredrich Michael Welter Heiko Rieger

September 27, 2018

Abstract

We explored the application of the adaption algorithm introduced by Secomb et. al. to artificial blood vessel networks and find that the resulting networks to not obey Murray's law. The reported analysis and visual examples document the contrast of the 2 types of networks. We conjecture that an interrupt of a established signaling cascade could be a hallmark of solid vascular tumors.

Contents

1 Introduction **3**

2 Methods **3**
2.1 The adaption algorithm . . . 3
2.2 The artificial blood vessel networks. . . . 4
2.3 Particle Swarm optimization . . . 4

3 Results **5**
3.1 Convergence . . . 5
3.2 Signal distribution . . . 5
3.3 Murray's law . . . 5
3.4 Quantitative analysis . . . 14

4 Discussion **14**

5 Conclusion **16**

A Reproducing available data **17**

1 Introduction

Physicists have always been fascinated by nature with its perfect shapes optimized by years of evolution to fulfill diverse range of tasks.

Nowadays, a lot of models follow the idea of activator and inhibitor as introduced by the famous paper of Turing in 1952 ([Tur52]). The sophisticated review [KM94] documents a lot of ideas where the quantitative predictions of Turings model are used to explain multiple patterns.

But even before, Cecil Murray proposed a model [Mur26] to describe her observations as biologist on blood vessel networks. She found that the cube of a parent vessel's radius equals the sum of the cubes of the daughter vessel's radii. Later this law was generalized (see equation 1, compare figure 1) and used not only for blood vessel networks, but for all kind of transport networks [She81]. Certainly the application of Murray's law culminates in the production of bio material based on the formula [ZSW+17].

$$r_c^\alpha = r_a^\alpha + r_b^\alpha \tag{1}$$

Nevertheless its superior application to networks with a strong hierarchy, the formula differs when hierarchy is present but less pronounced e.g. for the microvascular or the vascular bed. Beginning with their first paper in 1995 [PSG95], Pries and Secomb et. al. published a series of papers where they proposed a new way to regulate the radii in the vascular including the microvascular. We describe this model in the main part (section 2.1).

Later, others ([MAC06], [MMA+09]) included the adaption algorithm into their study of cancer.

In this work we focus the application of the adaption algorithm to artificial arterio venous networks created by *tumorCode* [FWR18].

2 Methods

2.1 The adaption algorithm

In [PSG98], the authors present a way to regulate vessel radii within arterio- venous networks which is numerically accessible. They construct a feedback loop between the spatial position of the vessels (topology) and their functions including hydrodynamics, shear stress and metabolism of of surrounding tissue.

For an elaborated review and some applications of the method contact [SDP12]. We briefly summarize the 5 signals forming the key elements of the algorithm.

S1 - Shear stress A vessel is supposed to shrink whenever the wall shear stress falls below $1 dyne/cm^2 = 10^{-4} kPa$ and expanding otherwise. When using *dyne* as unit, the logarithm offers the right dependence.

$$S_1 = \log_{10}(\tau_\mathrm{w}) \tag{2}$$

S2 - Pressure The second signal is created by the force acting on a vessel wall. To this end the authors of [PSG98] used a heuristic dependence obtained in their preceding publications. Due to the lack of better knowledge, we apply this formula as well.

$$S_2 = -\log_{10}\left(100 - 86\exp\left[-5000\left\{\log_{10}\left(\log_{10}(P)\right)\right\}^{5.4}\right]\right) \tag{3}$$

S3 - Metabolic demand The mathematical structure of S3 leads to expansion for small vessels with higher metabolic demand ($Q_\mathrm{ref} > HQ$) i.e. the capillaries and decrease for regions which exceed the reference flow ($Q_\mathrm{ref} < HQ$) i.e. big veins .

$$S_3 = k_\mathrm{m} \log_{10}\left(\frac{Q_\mathrm{ref}}{HQ}\right) \tag{4}$$

k_m is a model constant (compare table 1) and a priori not known. The introduced reference flow is biologically motivated by a minimal flow of RBCs which should always be maintained.

S4 - Topological position S_4 gives rise to the position of the vessels within the entire network structure. It is propagates from the place where the vessels interact most with the surrounding tissue: the capillary bed. While the downstream propagation from a capillary to a draining root transports consumed chemicals away from there place of interaction, the upstream signaling is less obvious. However recent studies confirmed that vessels send electrical signals within their endothelial layer.

We look at a single Y-shaped intersection and label the vessels with a,b,c. In the arterial branch a mother vessel has two downstream vessels whereas in the venous branch a daughter vessel has two upstream mothers respectively. The signal is calculate in a recursive fashion by

$$S_c = S_{3,a} + S_{3,b} + S_{4,a}\exp(-x_a/L) + S_{4,b}\exp(-x_b/L) \tag{5}$$

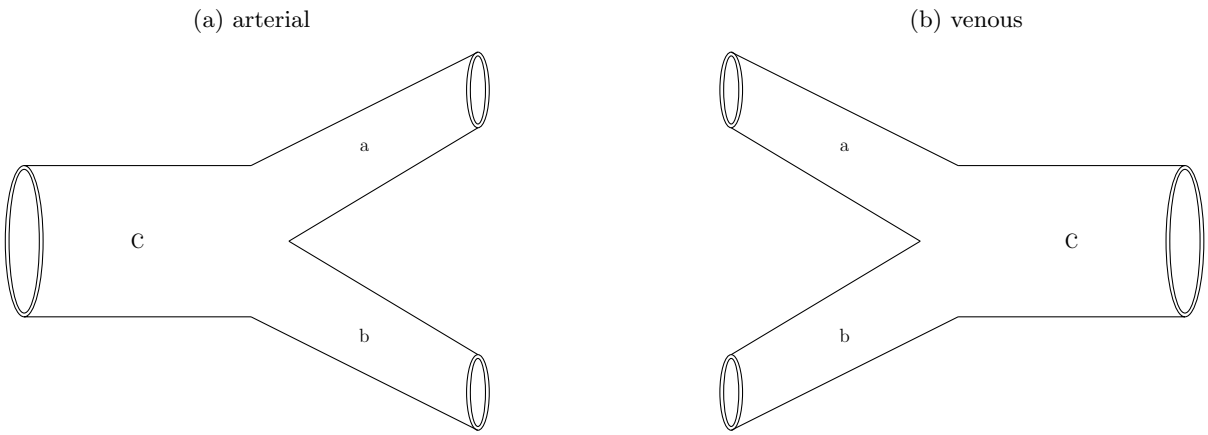

Figure 1: Illustration of the conductive signal propagation. Left column: arterial case. Right column venous case. Note that the direction in which the information is propagated is different. See text and Eq. 5.

The length of the segments (x_a and x_b) is normalized by an arbitrary model parameter L in the exponential. To account for possible nonlinearities, the saturation response to a reference value S_0 is used so that the total signal becomes

$$S_4 = k_{\mathrm{c}} \frac{S_c}{S_c + S_0} \tag{6}$$

Note that k_{c}, S_0 and L are unknown model parameters (compare table 1).

S5 - Shrinking tendency The authors propose that vessels will shrink in the absence of any other stimulation. This is embedded by subtracting a overall constant k_{s}.

$$S_5 = -k_{\mathrm{s}} \tag{7}$$

Response of single vessel The total signal at a vessel is the sum of the components and the change in radius becomes

$$\boxed{\Delta r = S_{tot}\ r\ \Delta t} \text{ with } S_{tot} = \sum_{i=1}^{5} S_i \tag{8}$$

2.2 The artificial blood vessel networks.

Since the adaptation algorithm was designed to work on experimentally measured topologies, it gives no further instructions on how to choose the spatial arrangement of the segments in question. Our software [FWR18] allows to construct artificial 3D arterio- venous networks. We report the complete methodology in [RFW16] and summarize the main steps here.

First, at least one arterial and one venous root node have to be distributed and assigned with either a blood pressure value or a flow rate. By using a hierarchical iteration scheme, the distribution of capillaries within the given space is optimized. Since the resulting radii are are governed by murrays law, we will call them **M-networks** from now on.

For the scope of this paper, we consider "Rootnode Configuration 4" (RC 4) where one artery is opposite one vein on the x-axis (Compare RC4 in figure 4 of [WFRR16]).

To conduct our studies we keep the topology of the **M-network**, and adapt the vessel radii accordingly to the model described in section 2.1. For reference we will call successfully adapted networks **A-networks** from now on.

2.3 Particle Swarm optimization

Inspecting section 2.1 we find 6 unknown parameters for the model, summarized in table 1. Considering the additional hydrodynamic boundary conditions for the root nodes, this are too many degrees of freedom to handle. Since we use the described model in different place, there is no hope that we can apply the parameters obtained by fitting to rat mesentery. However, the published parameters give us a guess about the dimension. We decide to adapt the values of $Q_{\mathrm{ref}} = 40$, $L = 1500$ and $S_0 = 20$ without change and and conduct a particle swarm optimization in the range of 0.5 to 4.0 for the other parameters. As reasonable biological objective we choose to minimize the variance of the capillary flow.

The hydrodynamic boundary conditions at the inlet and outlet of the network needs to be fixed before the optimization. We varied the outlet pressure between $0.5 - 9.0kPa$ and the inlet flow from $10^7 - 10^8 \mu m^3/s$ to cover a biological relevant range and optimized on a standard computing cluster using 20 Nodes and 320 CPUs. The implementation

signal	parameters	parameters fixed by [PSG98]
S_3	k_m	Q_{ref}
S_4	k_c	L, S_0
S_5	k_s	

Table 1: Free parameters of the model. The values in the right column are copied from the cited publication.

label	k_m	k_c	k_s
I	0.83	2.74	1.79
II	0.63	3.19	1.57
III	0.97	2.85	1.79

Table 2: Parameters used to apply the adaption to the artificial blood vessel networks.

uses the python packages deap ([FRG+12]) and Scoop ([HGGP14]) to fully utilize the parallel nature of particle swarm optimization. Details can be obtained from the complete source code at https://github.com/thierry3000/tumorcode

After we successfully determined the convergent range of boundary conditions, we chose a pressure of $2.8kPa$ at the venous outlet and a flow of $2e7\frac{\mu m^3}{s}$ and applied the adaption algorithm to 10 independent realizations of RC 4 networks of size $1500\mu m^3$ with 1 hierarchical iteration.

Inspired by the parameter set I, II and II in [PSG98], we applied the adaption procedure to the 10 independent samples with the following parmeters reported in table 2.

3 Results

After successfully recover the results on a measured data set (see section A), we subsequent identified boundary conditions where the optimization converged and created an ensemble 10 **A-networks** s.

3.1 Convergence

As discussed in [PSG98], there are 2 possible outcomes if one applies the adaption scheme in a repeated manner: either one reaches an equilibrium steady state where the changes of radii become arbitrary small with increasing iteration or the changes increase to unrealistic values which also implies unrealistic values for pressure and flow.

By systematic variation (particle swarm optimization 2.3) of the hydrodynamic boundary conditions, we identified areas where the adaptation algorithm converges and defined the parameter regime to study. The convergent regions can be appreciated in Fig. 2. In total we find 253 convergent sets of boundary conditions. Each convergent set gives rise to the best choice for parameters in question which are k_m, k_c and S_5. The associated distribution is summarized by a box plot in Fig 3.

3.2 Signal distribution

Akin to figure 13 and 14, we plot for sample with id no. 5: a) the conductive and metabolic signals in figure 4; b) the hydrodynamic signal in figure 5; and c) the hydrodynamic characteristics in figure 6. Due to the construction of the signaling cascade and the convergence of the algorithm, we are not surprised that the distributions of the signals look qualitatively similar.

However the radii change from the **M-networks** (bottom left figure 7) to **A-networks** (bottom right column of figure 7), the upper row shows that the pressures do no change because of the fixed boundary conditions. Since the adaption changes the radii, the flow needs to be modified accordingly! We model the shear force proportional to the flow so that differences between the images in the center row hold for the shear force and the flow simultaneously. In the bottom row we colored the vessel by their radii to highlight the result of the adaption algorithm.

In figure 8 we show the data that is only available for the adaption case. In agreement with model assumptions, the metabolic signal is highest at the thin capillaries and the conductive signal is highest at the most distal points.

3.3 Murray's law

By construction the **M-networks** fulfill Murray's law (equation 1). We found that **A-networks** do not fulfill Murray's law (see figure 9 and the inset).

Despite its simple appearance, the dependence in murray's law is tricky. In figure 10 we look at every possible intersection within the network and check the differences between left and right branch for a representative of **M-networks** (in the left panel) and a representative of **A-networks** (in the right panel). We find that this distribution is smooth out by the adaption and becomes much broader (see absicca of figure 10).

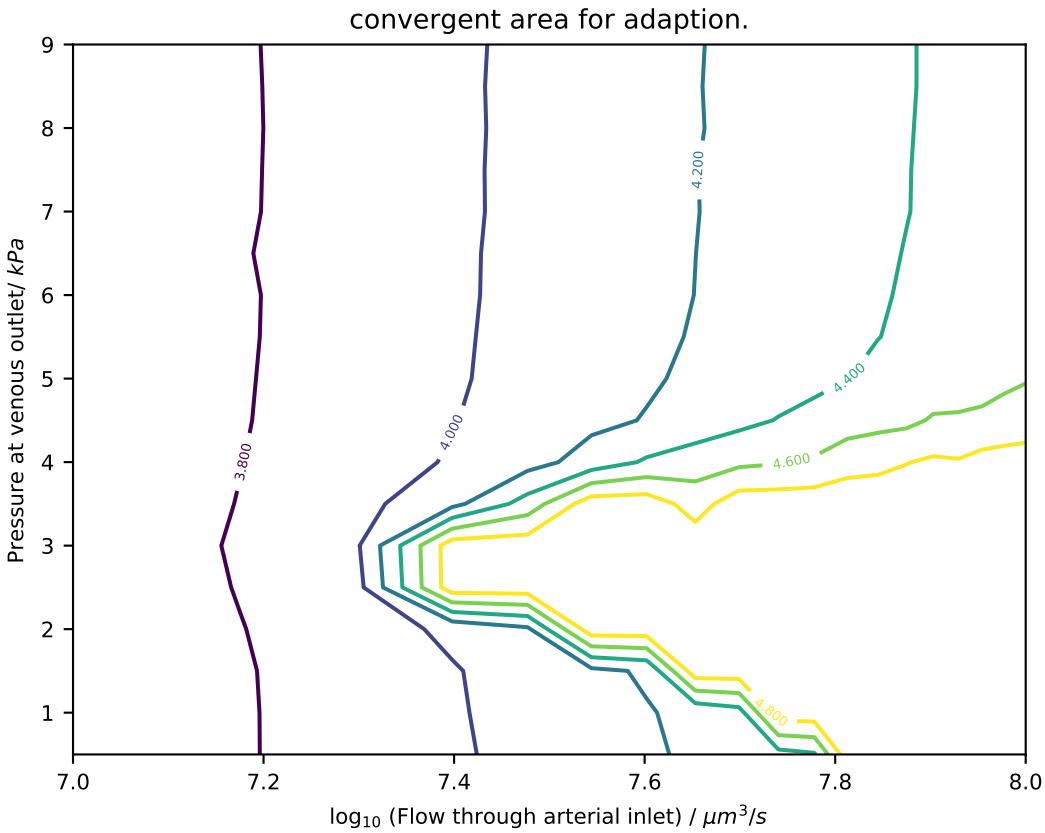

Figure 2: Contour plot showing the log_{10} of the fitness value from the particle swarm optimization i.e. the log_{10} of the standard deviation of the average capillary flow. The x- axis represents the boundary condition at the arterial inlet in logarithmic scale. The y- axis represents the boundary condition at the venous outlet.

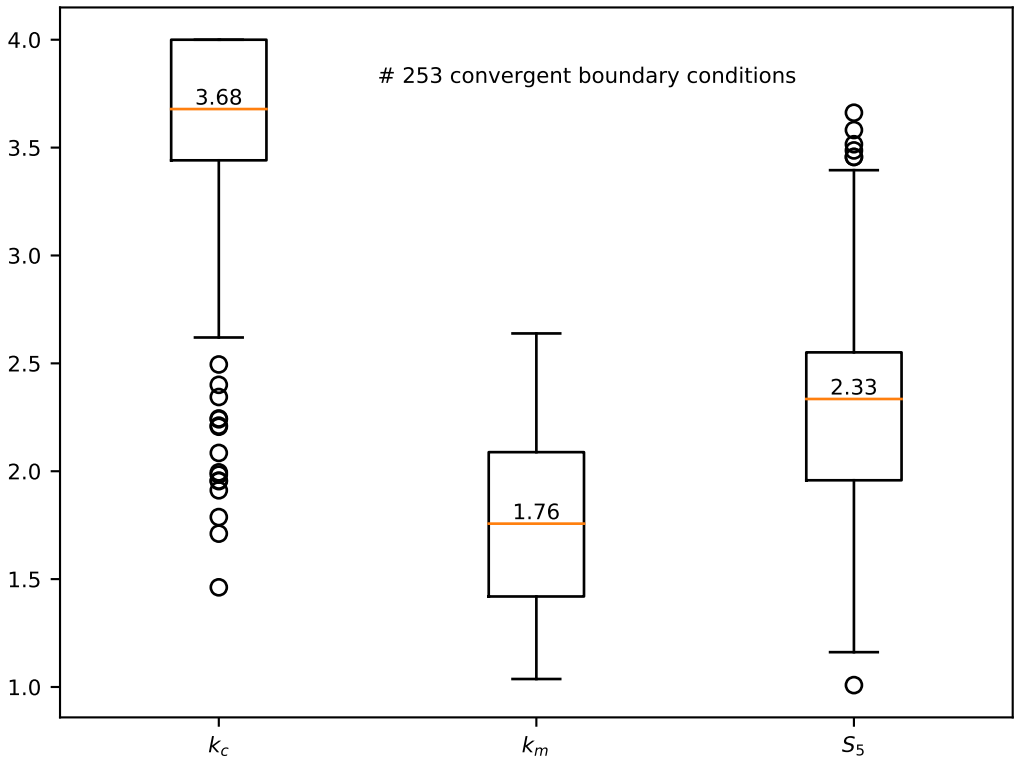

Figure 3: Boxplot summarizing the best choice for k_m , k_c and k_s as obtained by particle swarm optimization. Only convergent data sets are considered. The median value is write above the corresponding line.

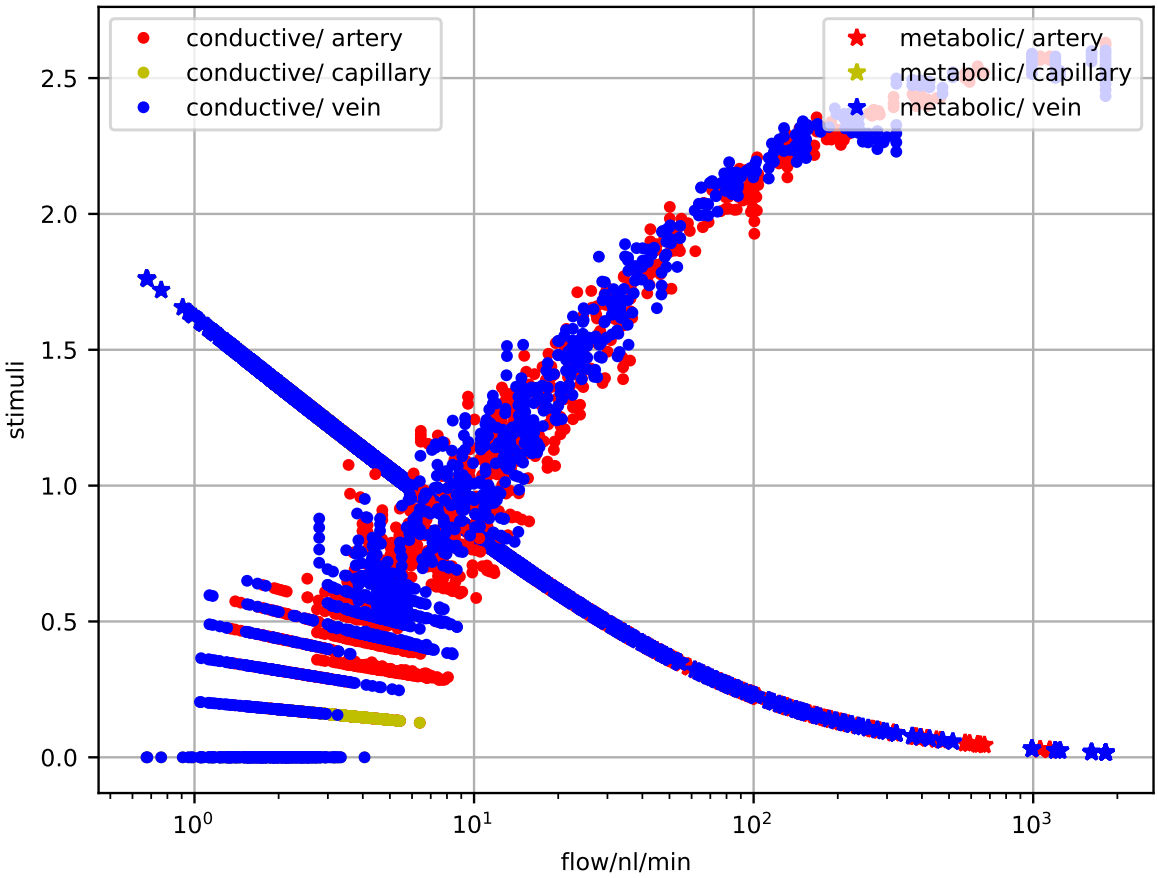

Figure 4: Akin to figure 5 lower row in [PSG98], this figure shows the strength of the adaption stimuli based on the conductive and the metabolic signal. Metabolic signals are indicated by asterisks and conductive signals by bullets. The color is based on the vessel type store by *tumorCode* .

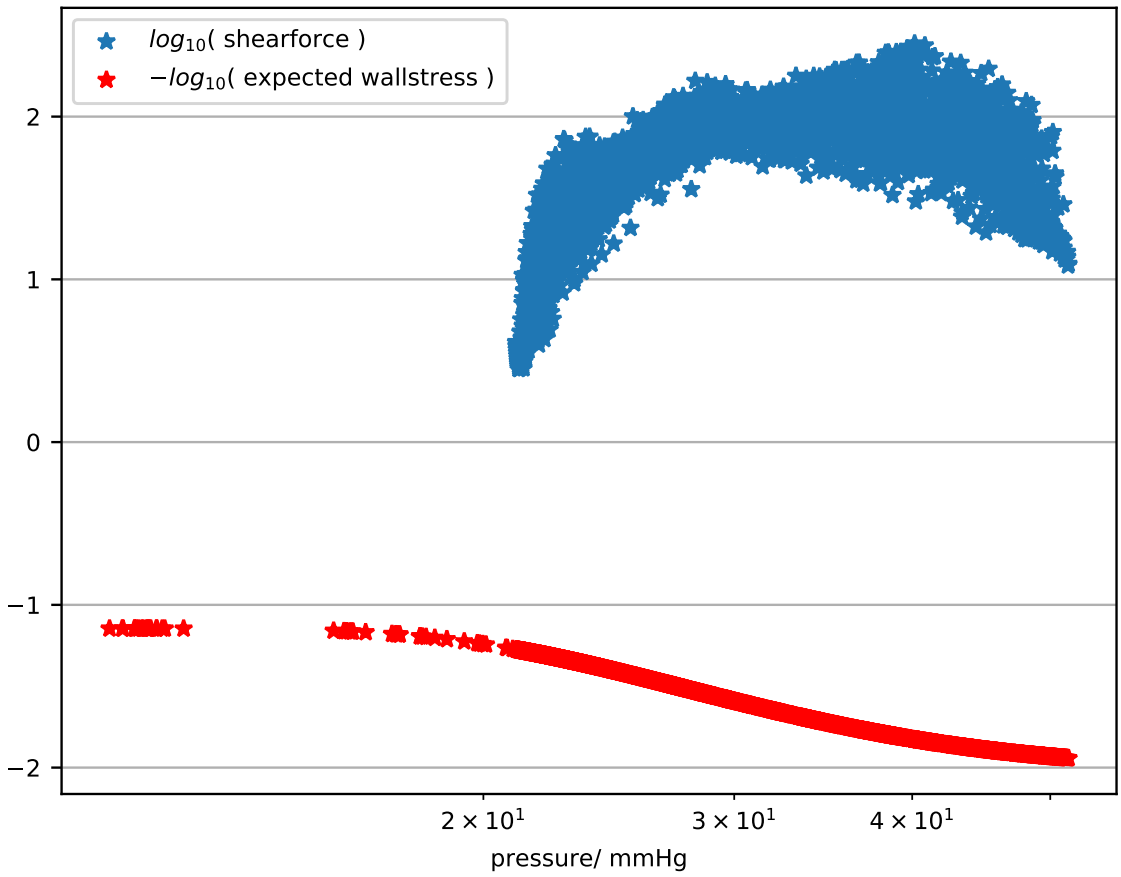

Figure 5: Akin to figure 5 B) in [PSG98], this figure shows the hydrodynamic stimuli derived from the shear force (τ_w) and the pressure P

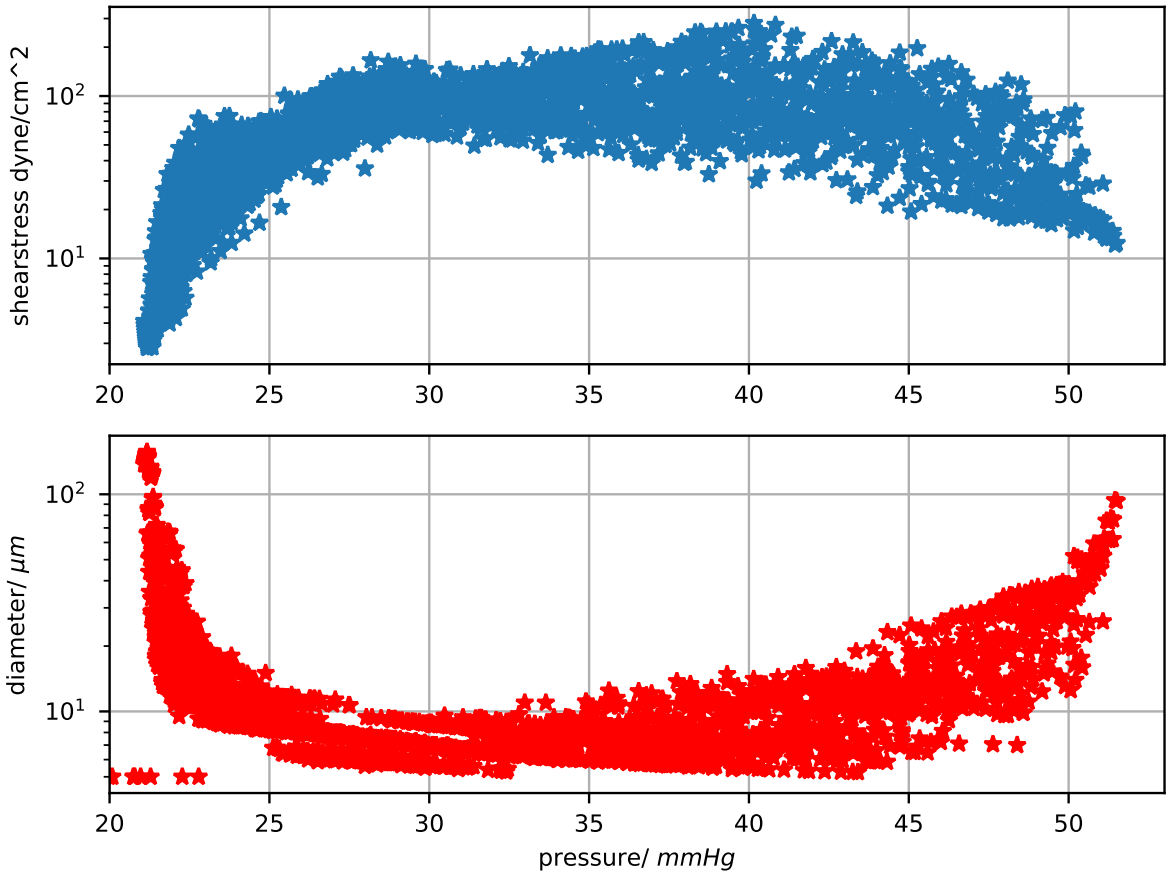

Figure 6: Akin to figure 4 lower row in [PSG98], this figure shows characteristic hemodynamic and morphological parameters of the **M-networks** with id 5. In the top row the acting shear stress is plotted along the vessels blood pressure. In the bottom row the vessel diameter is plotted along the vessels blood pressure.

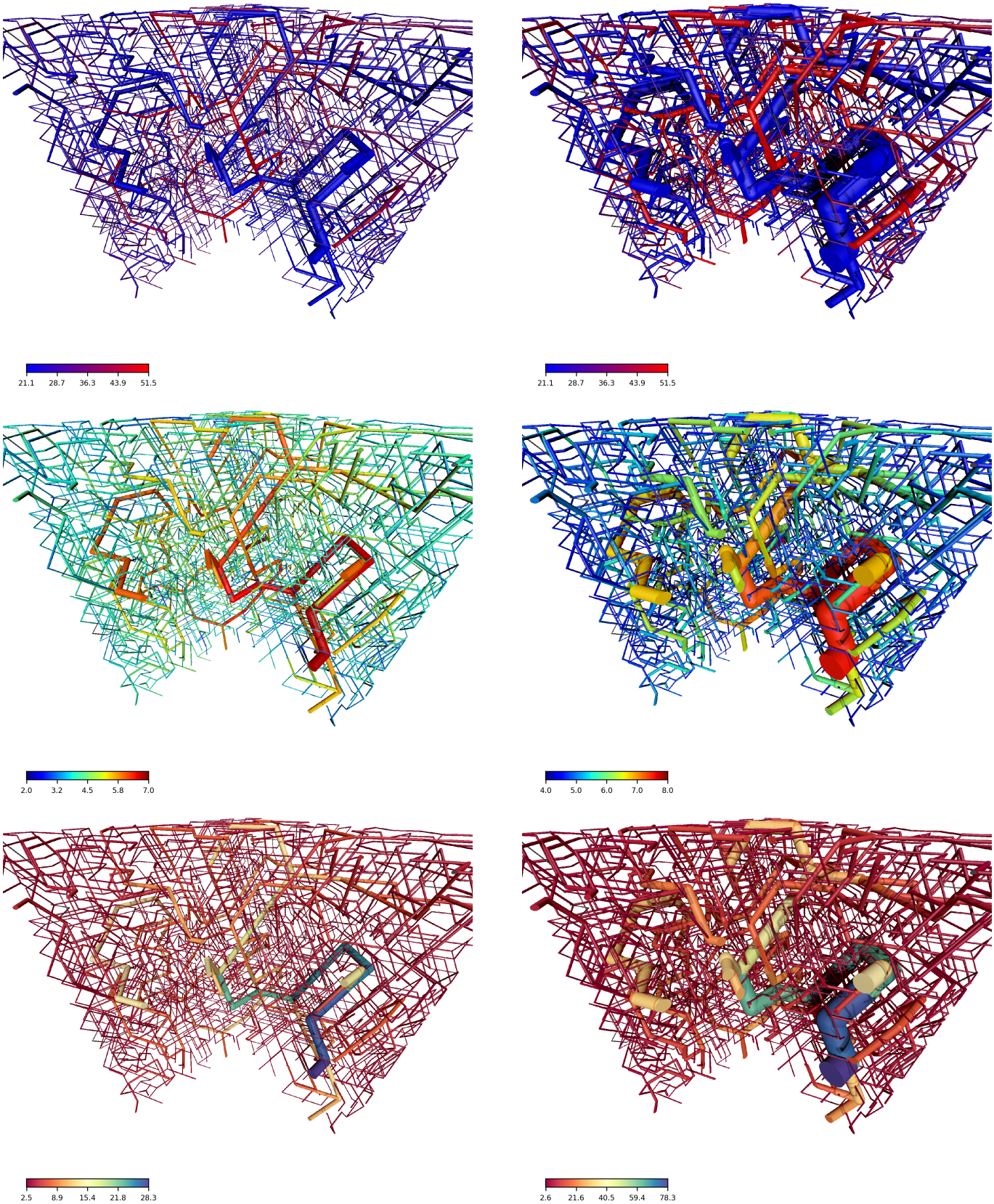

Figure 7: Color coded vessel properties for network with id 5. From top to bottom: pressure in $mmHg$, shear force in log, radius. Left column show the **M-networks** and the right column depict the **A-networks** .

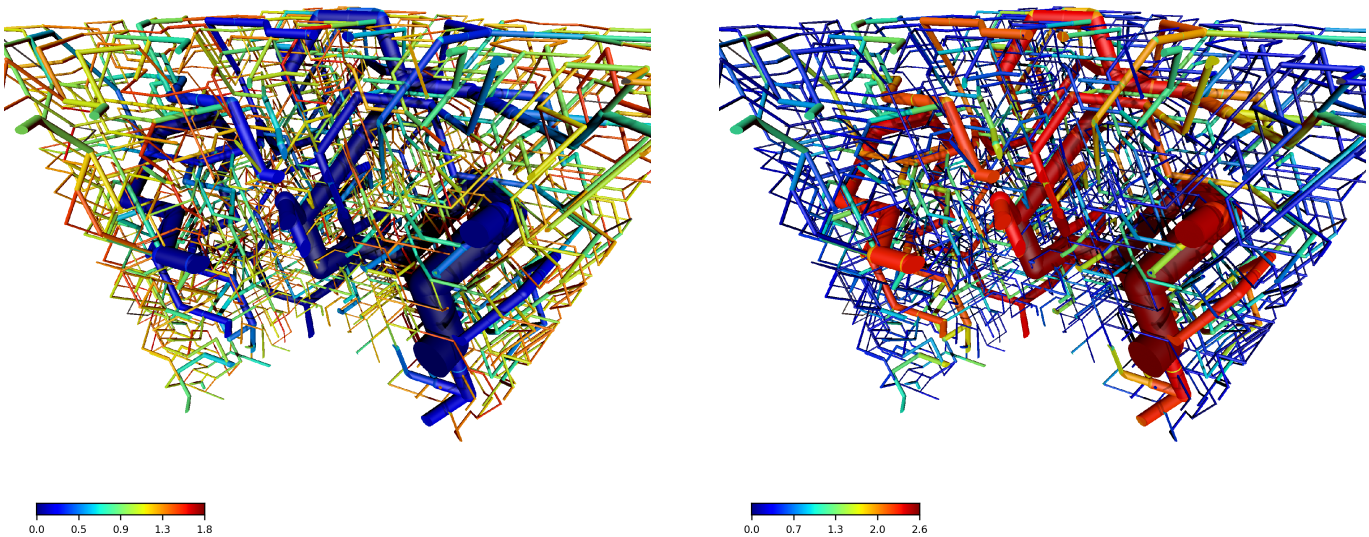

Figure 8: The figure shows vessel properties that are available in the adaption case for network with id 5. Left column: metabolic signal as calculated in equation 4. Right column: conductive signal as calculated in equation 5.

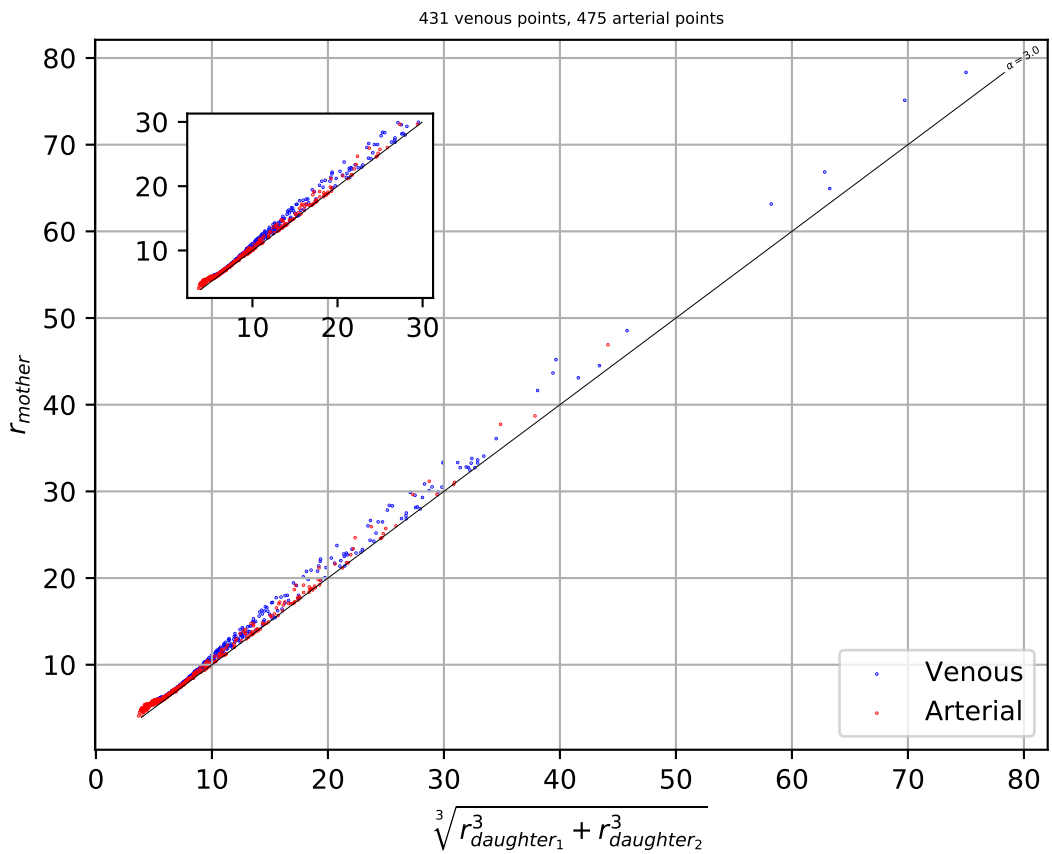

Figure 9: The black diagonal represents murray's law for $\alpha = 3$. The data points are taken from the convergent data set with id 5. Blue dots are venous intersections and red dots are arterial intersections. The inset shows the same curve at lower values (see axis).

(a) *tumorCode*

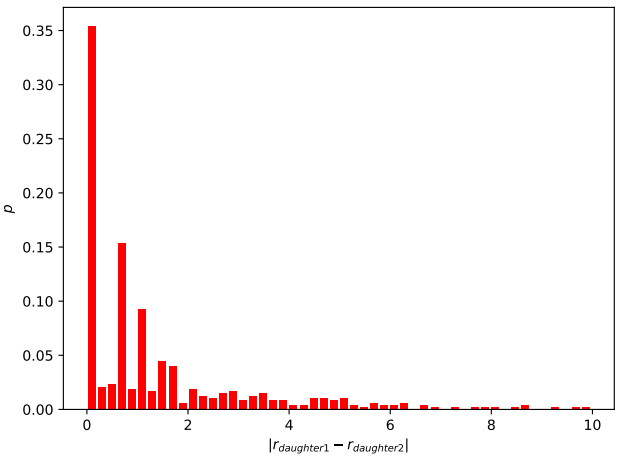

(b) adaptation

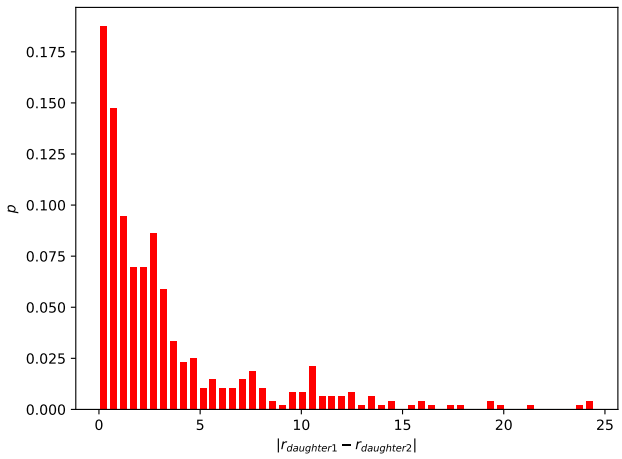

Figure 10: Normalized distribution of differences between two daughter vessels at a Y- shaped intersection. In both cases the representative with id 5 is used. Left column: **M-networks** . Right column: **A-networks** obtained with parameterset I.

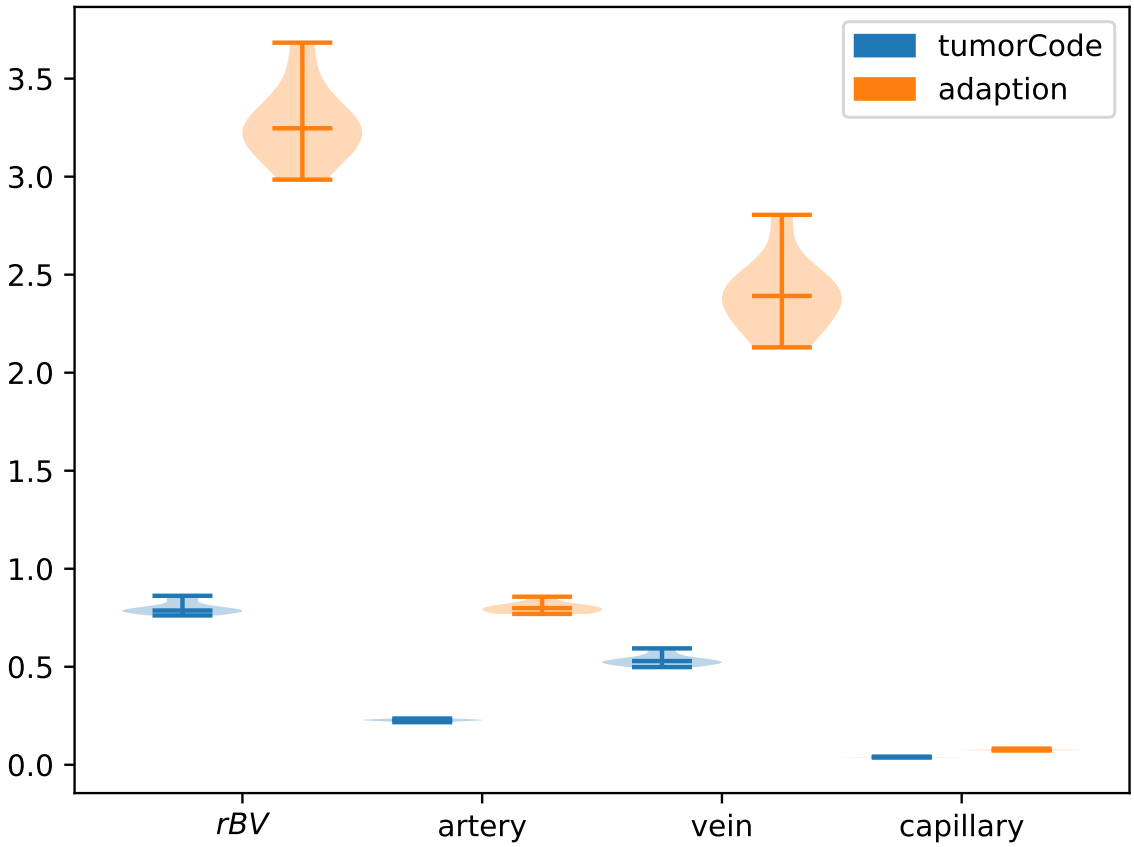

Figure 11: The reginal blood volume (rBV) is averaged over 10 network samples and shown by percent. From left to right the data for all vessels, only arteries, only veins and only capillaries is shown. The blue color is used for the M-networks before adaption and orange is used for the adapted networks. Note that artery, vein and capillary add up to the rBV entry.

3.4 Quantitative analysis

We determined the regional blood volume (rBV) and the surface to volume ratio for each of the 10 samples before (**M-networks**) and after the adaption (**A-networks**). For the **A-networks** , the rBV is more than 3 time higher than for the **M-networks** (see figure 11). While the contributions from arteries and veins vary significantly, the contribution from the capillaries are about the same.

Considering the surface to volume ratio (figure 12), *tumorCode* creates networks with a higher ratio resulting in a better biological efficiency. Note that the s2v ratio is highest for the capillaries in the M-networks.

We conclude that the optimization arranging the capillaries in *tumorCode* fulfills its purpose: namely to create a homogeneous environment for nutrient exchange.

4 Discussion

The algorithm in question (section 2.1) was designed to assess data sets obtained from animal models. Unfortunately such data is still very rare. We applied the the adaption scheme to artificial blood vessel networks obtained by *tumorCode* . In contrast to previous approached, we could not fit to measured data sets to obtain the free parameters (compare table 1) . Therefor we exploit PSO to estimate the parameters under reasonable assumptions which are a) biological boundary conditions (inflow and pressure at outlet) and b) homogeneous distribution of hydrodynamics within the capillary bed.

The radii of convergent data sets do not follow Murray's law (9 and 10) where two aspects of energy are included and balance to the famous formula. The concept of adaption includes more than two aspects of energy. Hydrodynamic energies are augmented by a form of electrical or topological energy (conductive signal) and chemical energies (metabolic signal) which have to be minimized mutually. From figure 7 and 8 in section 3.2 and the data in section 3.4 it becomes obvious how the the two presented types of vessel networks differ. A quantitative analysis of regional

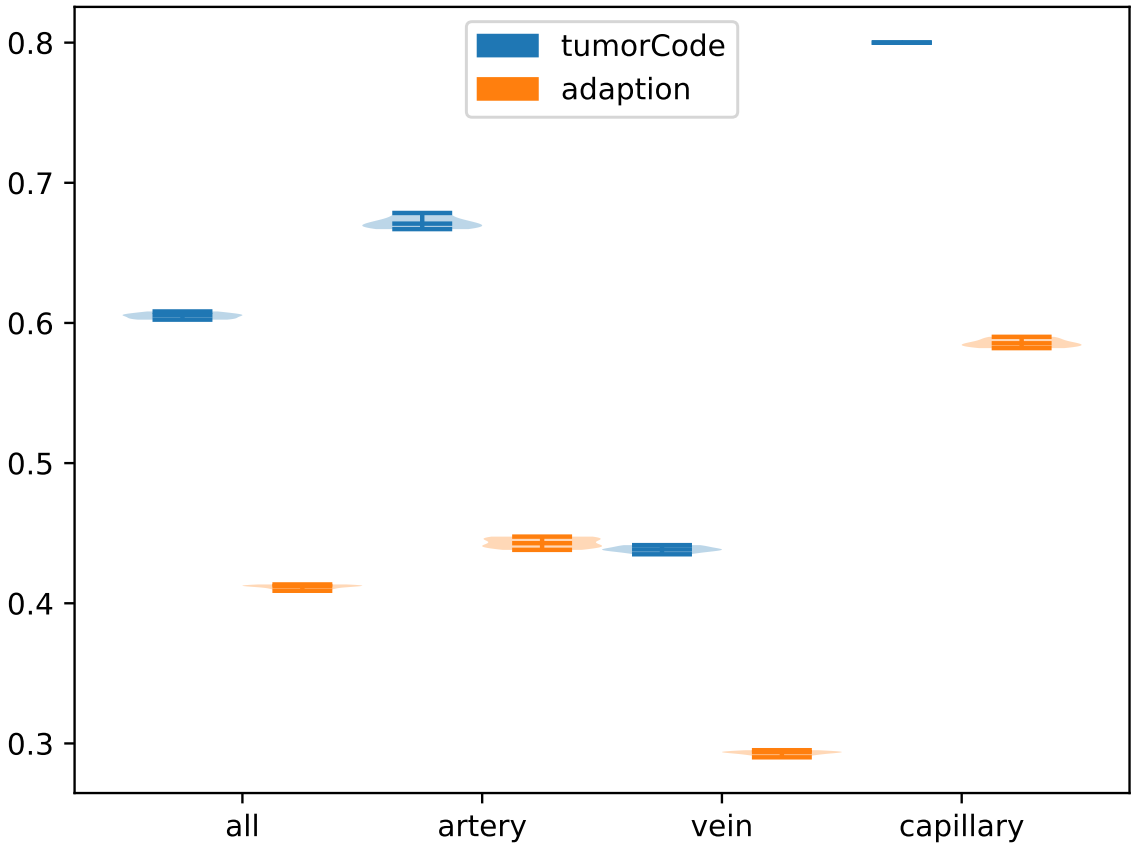

Figure 12: The surface to volume ratio (s2v) is averaged over 10 network samples. From left to right the data for all vessels, only arteries, only veins and only capillaries is shown. The blue color is used for the M-networks before adaption and orange is used for the adapted networks.

blood volume (rBV) and surface to volume ratio (s2v) showed that the **A-networks** carry more blood while the **M-networks** offer a higher surface to volume ratio — especially at the capillary level.

We failed adding the algorithm to the implementation of vascular tumor growth in *tumorCode* (data not shown). For a fixed set of adaption parameters, the convergence was not stable while vessel regression or angiogenesis happened. In those cases the conductive signal was interrupted or shared between new vessels and prevented convergence. Others who used the adaption algorithm in the realm of tumor growth resigned to use the conductive signal at all. We could not find an explanation why they neglected this in their work. In contrast, it is stated in [MAC06]:

> "These stimuli form a basic set of requirements in order to obtain stable network structures with realistic distributions of vessels diameters and flow velocities."

while Pries and Secomb [PSG98] stated that:

> "..., it is necessary to introduce a further stimulus that reflects the topological position of a segment in the networks, ..."

and

> "These tests confirmed that all four stimuli were needed to prevent strong strong deviations of ..."

Those facts let us worry about their results.

5 Conclusion

We applied the adaption algorithm introduced by Secomb et. al. in [PSG98] to synthetic arterio- venous networks. To our knowledge such an application was not done before because the selection of the free parameters was restricted to experimental data. In future, when computers become even more powerful, the application of non linear optimization techniques such as the presented particle swarm optimization will allow to retrace the construction of arterio- venous networks — and more questions occuring in nature.

The signals introduce by the adaption algorithm provide an intersection to the ever increasing understanding of basic biological processes and mathematical modelling. Currently the signals are modeled with parameters (the free parameters in our description, compare table 1), but what if those signals become experimentally accessible input in future? The model is ready and once the drop in voltage along a vessel or its metabolic uptake are measurable, we can fix the parameters.

In future, we hope to understand the feedback between vascular tumors, the adption signals and the topology of blood vessels in tissue.

k_c	2.74
k_m	0.83
k_s	1.99*
Q_{ref}	40
S_0	20
Δt	0.1*

Table 3: Parameter used to adapt radii of rat mesentery network with *tumorCode* . Parameters labeled by * are not the same as in the publication of [PSG98], see text.

(a) initial

(b) after convergence

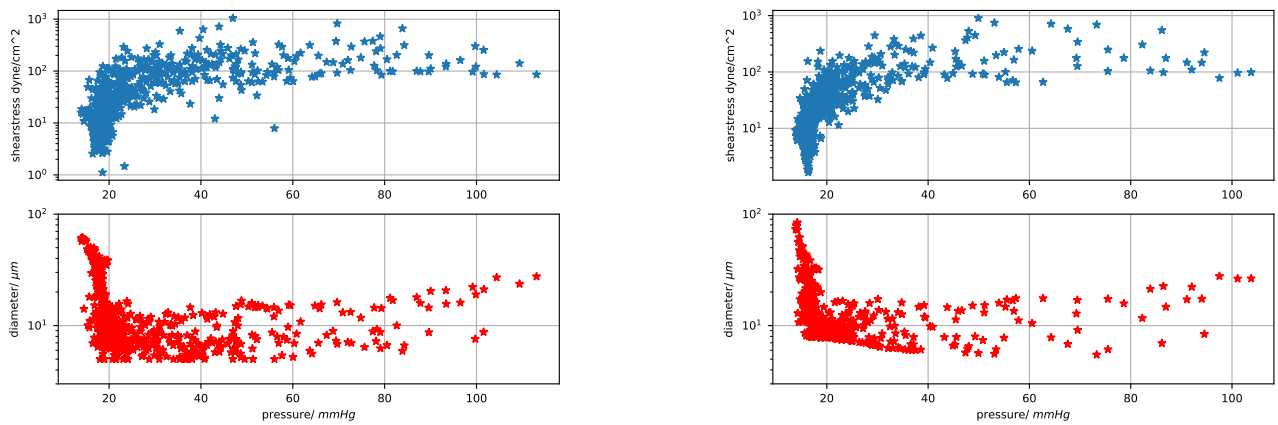

Figure 13: Distribution of characteristic hemodynamic and morphological parameters. Column a) before and column b) after convergent adaptation. The top row shows the shear stress as a function of the blood pressure. Lower row shows the vessel diameter likewise as function of the blood pressure. Note that the ordinate is on logarithmic scale.

A Reproducing available data

We applied our implementation of the adaption algorithm to the network published by Pries et al. [PSG98]. They measured the hydrodynamic boundary conditions which we incorporate accordingly. Unfortunately a differential time step is stated but not documented — we used $\Delta t = 0.1$. Furthermore it was not sufficient to use exactly the same parameters as documented Secomb et al. We achieve convergence we changed k_s from 1.79 to 1.99 in our simulations. We believe this required since our calculation of the hemodynamics is more advanced and therefore results in slightly different behavior.

To check our implementation we reproduced Fig. 4 and 5 of [PSG98]. Due to the lack of quantitative data, we cannot compare directly, but we find that Figure 13 is in qualitative agreement with its original.

Figure 14 (top row, left) lacks negative values for the logarithm of the shear force. Obviously our model does not include such a case.

The lower row of Figure 14 is in qualitative agreement with [PSG98]. Here we accomplished the plot with information about the type of vessels (artery, capillary or vein) which is required to use *tumorCode* .

(a) initial

(b) after convergence

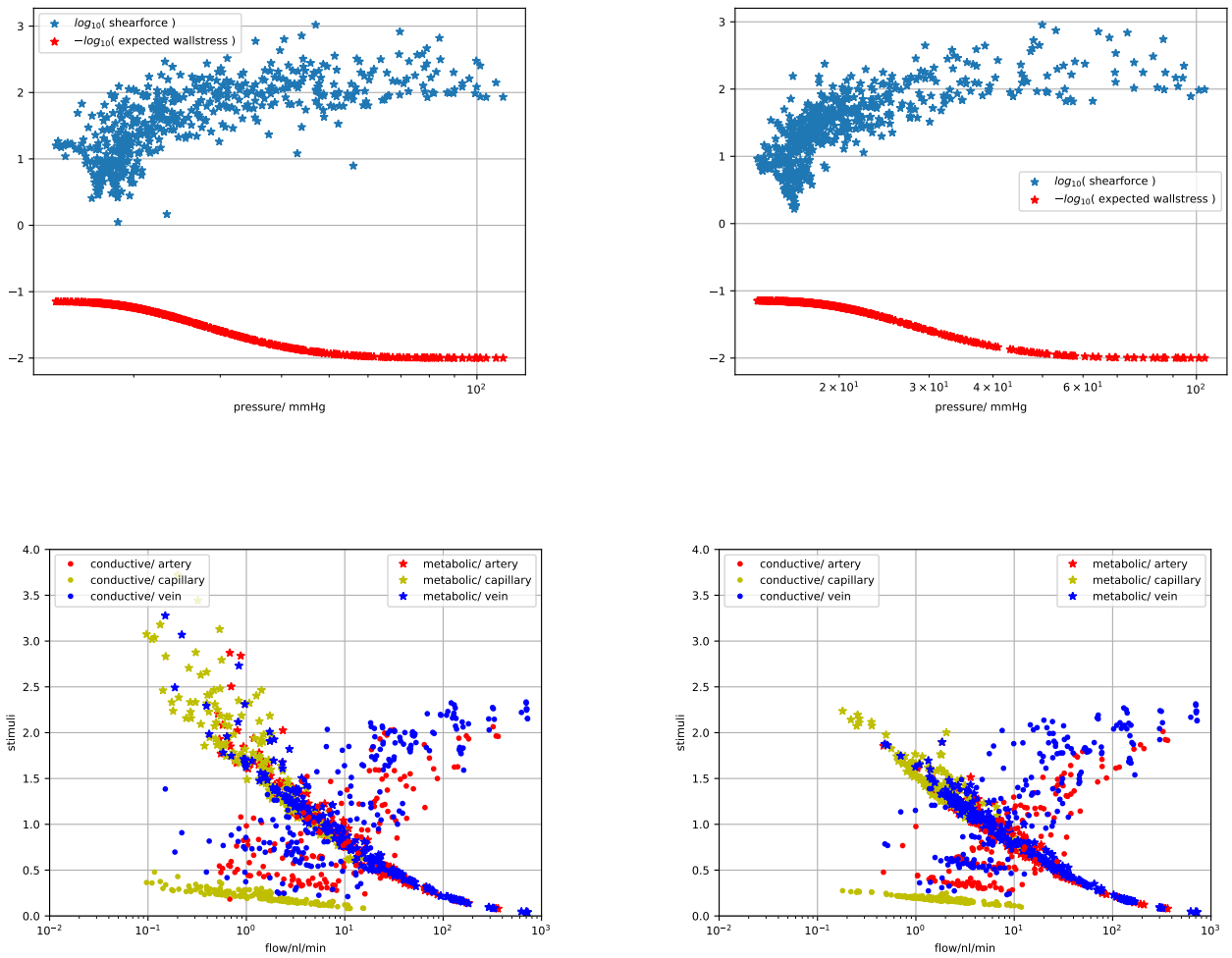

Figure 14: Signals contributing to the total adaptation signal of the rat mesentery network consisting of 546 segments. Left column shows the signal strength at the beginning of the adaptation procedure and the right column the situation once convergence is reached. Upper row depicts the hydrodynamic parts of the signal. S_1 derived from the shear force in blue. S_2 derived from the transmural pressure in red. Lower row depicts the metabolic and conductive parts which corresponds to S_3 and S_4. Colors interpret the type of the vessel which could be either artery, vein or capillary.

References

[FRG+12] Félix-Antoine Fortin, François-Michel De Rainville, Marc-André Gardner, Marc Parizeau, and Christian Gagné. DEAP: Evolutionary Algorithms Made Easy. *Journal of Machine Learning Research*, 13:2171–2175, July 2012.

[FWR18] Thierry Fredrich, Michael Welter, and Heiko Rieger. Tumorcode. *Eur. Phys. J. E*, 41(4):55, April 2018.

[HGGP14] Yannick Hold-Geoffroy, Olivier Gagnon, and Marc Parizeau. Once You SCOOP, No Need to Fork. In *Proceedings of the 2014 Annual Conference on Extreme Science and Engineering Discovery Environment*, XSEDE '14, pages 60:1–60:8, New York, NY, USA, 2014. ACM.

[KM94] A.J. Koch and Hans Meinhardt. Biological Pattern-Formation—From basic mechanisms to complex structures. *Reviews of Modern Physics*, 66:1481, October 1994.

[MAC06] Steven R. McDougall, Alexander R. A. Anderson, and Mark A. J. Chaplain. Mathematical modelling of dynamic adaptive tumour-induced angiogenesis: Clinical implications and therapeutic targeting strategies. *Journal of Theoretical Biology*, 241(3):564–589, August 2006.

[MMA+09] Paul Macklin, Steven McDougall, Alexander R. A. Anderson, Mark A. J. Chaplain, Vittorio Cristini, and John Lowengrub. Multiscale modelling and nonlinear simulation of vascular tumour growth. *J. Math. Biol.*, 58(4):765–798, April 2009.

[Mur26] Cecil D. Murray. The Physiological Principle of Minimum Work. *Proc Natl Acad Sci U S A*, 12(5):299–304, May 1926.

[PSG95] A. R. Pries, T. W. Secomb, and P. Gaehtgens. Design principles of vascular beds. *Circ. Res.*, 77(5):1017–1023, November 1995.

[PSG98] A. R. Pries, T. W. Secomb, and P. Gaehtgens. Structural adaptation and stability of microvascular networks: theory and simulations. *American Journal of Physiology - Heart and Circulatory Physiology*, 275(2):H349–H360, August 1998.

[RFW16] Heiko Rieger, Thierry Fredrich, and Michael Welter. Physics of the tumor vasculature: Theory and experiment. *Eur. Phys. J. Plus*, 131(2):31, February 2016.

[SDP12] Timothy W. Secomb, Mark W. Dewhirst, and Axel R. Pries. Structural Adaptation of Normal and Tumour Vascular Networks. *Basic Clin Pharmacol Toxicol*, 110(1):63–69, January 2012.

[She81] T. F. Sherman. On connecting large vessels to small. The meaning of Murray's law. *The Journal of General Physiology*, 78(4):431–453, October 1981.

[Tur52] Alan Mathison Turing. The chemical basis of morphogenesis. *Phil. Trans. R. Soc. Lond. B*, 237(641):37–72, August 1952.

[WFRR16] Michael Welter, Thierry Fredrich, Herbert Rinneberg, and Heiko Rieger. Computational Model for Tumor Oxygenation Applied to Clinical Data on Breast Tumor Hemoglobin Concentrations Suggests Vascular Dilatation and Compression. *PLOS ONE*, 11(8):e0161267, August 2016.

[ZSW+17] Xianfeng Zheng, Guofang Shen, Chao Wang, Yu Li, Darren Dunphy, Tawfique Hasan, C. Jeffrey Brinker, and Bao-Lian Su. Bio-inspired Murray materials for mass transfer and activity. *Nature Communications*, 8:14921, April 2017.